STARS

Honors Undergraduate Theses

UCF Theses and Dissertations

2021

Bicycle Wheel Aerodynamics Predictions Using CFD: Efficiency Using Blade Element Method

Drew Vigne
University of Central Florida

Showcase of Text, Archives, Research & Scholarship

BICYCLE WHEEL AERODYNAMICS PREDICTIONS USING CFD:

EFFICIENCY USING BLADE ELEMENT METHOD

by

DREW VIGNE

A thesis submitted in partial fulfillment of the requirements

for the Honors in the Major Program in Mechanical Engineering

in the College of Engineering and Computer Science

and in the Burnett Honors College

at the University of Central Florida

Orlando, Florida

Spring Term, 2021

Thesis Chair: Michael Kinzel, Ph.D.

ABSTRACT

The cycling industry has long relied on expensive wind tunnel testing when designing aerodynamic products, particularly in the context of wheels which account for 10 to 15 percent of a cyclist's total aerodynamic drag. With the recent advent of Computational Fluid Dynamics (CFD), the industry now has an economical tool to supplement the wheel design process; however, the complex nature of rotating spoked wheels requires high resolution meshes to model at acceptable fidelity. This research investigates an alternative CFD method that lowers the computational cost of modeling aerodynamic bicycle wheels by modeling spokes using Blade Element Method (BEM). Two CFD models of a HED Trispoke wheel, one with resolved spokes and one with modeled spokes, are compared to existing CFD and wind tunnel drag coefficient data at various headwind speeds and yaw angles. Data shows good agreement.

TABLE OF CONTENTS

LIST OF FIGURES

LIST OF TABLES

NOMENCLATURE

CFD	Computational Fluid Dynamics	
BEM	Blade Element Method	
MT	Momentum Theory	
BET	Blade Element Theory	
2D	Two-Dimensional	
3D	Three-Dimensional	
Re	Reynolds Number	
AoA	Angle of Attack	
RANS	Reynolds Averaged Navier Stokes	
SA	Spalart-Allmaras	
V	Bicycle Speed	
V_e	Effective Velocity	*V*cos(Yaw Angle)*
x'y'z'	Wheel Local Coordinate System	
$F_{x'}$	Drag Force	
$F_{y'}$	Vertical Force	
$F_{z'}$	Side (Lift) Force	
ρ	Air Density	
D	Wheel Diameter	
R	BEM Outer Radius	
r	BEM Local Radius	
S	Wheel Reference Area	*$\pi D^2/4$*
Cd	Drag Coefficient	*$F_{x'}/0.5\rho V^2 S$*
Cs	Side (Lift) Coefficient	*$F_{y'}/0.5\rho V^2 S$*
Cv	Vertical Coefficient	*$F_{z'}/0.5\rho V^2 S$*
w	Wheel Rotational Velocity	*V/0.5D*
p	Pressure	
τ	Viscous Stress Tensor	
b	Momentum Source Vector	
u	Velocity Vector	
$\tilde{v}$	SA Modified Diffusivity	
d	Length Scale	
r'	Normalized Disk Span	

ACKNOWLEDGEMENTS

Chapter 1: Introduction

Background and Objectives

Elite sports like professional cycling oftentimes have victories decided by the slimmest of margins. Take the 2020 Vuelta a España for example, where cyclist Primož Roglič beat competitor Richard Carapaz by a mere 24 seconds after 72 hours of racing 18 stages. This was a time gap of less than 0.01 percent and exhibits a perfect example where marginal aerodynamic gains could have altered an outcome. Previous works have established that on level ground at speeds over 25 mi/h, 90 percent of a cyclist's mechanical power output is required to overcome aerodynamic drag (Grappe et al., 1997; Kyle and Burke, 1984). Because of this, engineers and cyclists have mutually recognized that aerodynamics optimization is key to winning races, especially when a cyclist is in a position where they cannot take advantage of drafting, such as in breakaways or time trials. Previous works show that the three dominating sources of a cyclist's aerodynamic drag are cyclist posture, frame, and wheels, with the wheels accounting for 10 to 15 percent of the total (Greenwell et al., 1995). Wheels with aerodynamic features such as elliptical rims and spokes have shown to reduce total aerodynamic drag on the order of 2 to 3 percent when compared to conventional wheels. Therefore, it is worthwhile to invest in bicycle wheel aerodynamics optimization.
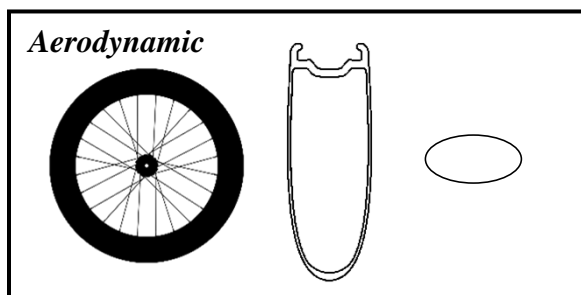
Figure 1: Zipp 808 Sideview, Rim Cross-Section, and Spoke Cross-Section
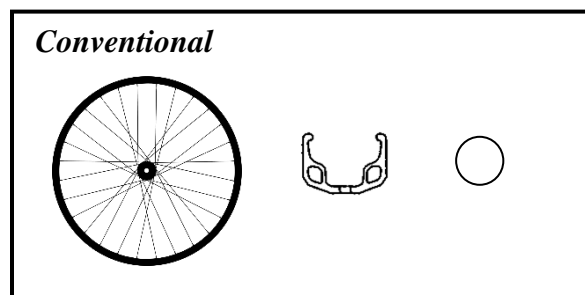
Figure 2: Conventional Wheel Sideview, Rim Cross-Section, and Spoke Cross-Section

Efforts to optimize aerodynamic bicycle wheels typically involves investing hundreds of thousands of dollars into wind tunnel testing; however, CFD is becoming an increasingly popular supplemental design tool. Documentation states that wheel manufacturer Zipp spends $850 per hour for 250 to 340 hours per year (Godo et al., 2010) and other sources claim $5000 to $10,000 per day (Debraux et al, 2011). Godo explains that Zipp uses CFD to narrow down from 100 wheel designs to 10, and then chooses the best design from among these 10 based on data from the wind tunnel. This is an increasingly popular iterative design practice in the cyclist industry – taking advantage of the wind tunnel's precision while simultaneously exploiting CFD's ability to rapidly iterate at a relatively low cost. In his own work, Godo compares CFD and wind tunnel aerodynamics predictions of several different bicycle wheels, including the Zipp 404, Zipp 808, Zipp 1080, and the HED Trispoke (Godo et al., 2009; Godo et al., 2010; Godo et al., 2011). Most notably, Godo is able to capture drag coefficient and side (lift) coefficient data for each of these wheels at high fidelity, producing data trends that are in good agreement to existing wind tunnel data.

High fidelity CFD typically requires a high density mesh, which means simulations take a long time to converge and hence have a high computational cost. This is particularly true when dealing with geometries that have fine detail relative to neighboring meshed bodies, such as bicycle wheel spokes compared to the rest of the wheel. A highly refined mesh is often required to fully resolve forces and induced velocities in the spoke region between the rim and hub, which effectively drives up computational cost. The scope of this work seeks develop an approach that models spokes instead of fully resolving them, thus lowering the computational cost of CFD involving bicycle wheels. Essentially a spoke is a kind of blade, therefore the spokes can be thought of as a kind of rotor. The authors of this work believe that BEM can be applied to spokes

just like the method is applied to wind turbine or helicopter rotors. BEM has historically been used to lower the computational cost of this type of CFD by requiring a relatively low density mesh without sacrificing simulation fidelity. In the context of bicycle wheel aerodynamics predictions, this could mean a faster and therefore more economical iterative design process for engineers in the cycling industry.

Chapter 2: Approach

Overview of Blade Element Method

BEM is one of the oldest and most used methods for calculating induced velocities and forces on rotors like those of wind turbines or helicopters. In the commercial code Star-CCM+, BEM is implemented as the combination of two methods, Momentum Theory (MT) and Blade Element Theory (BET).

MT relies on classical Newtonian mechanics to gain insight into parameters like disk loading and power required per pound of thrust (Yaggy et al., 1973). Essentially MT assumes that the pressure drop or loss of momentum in the rotor plane is caused by the work done as the airflow passes through the rotor plane (Moriarty and Hansen, 2000), which allows for calculation of tangential and axial induces velocities. While this approach does provide some insight into wholistic rotor aerodynamics, it fails to account for the unique properties of the individual blades such as blade airfoil characteristics. Therefore, it is necessary to couple this approach with BET.

BET overcomes the limitations of simple MT by introducing the unique properties of the individual blades into the algorithm. Essentially BET assumes that the rotor blades can be divided up into small elements that act independently of surrounding elements and operate aerodynamically as two-dimensional (2D) airfoils whose aerodynamic forces can be calculated based on local flow conditions (Moriarty and Hansen, 2000). It divides the blade elements up tangentially and axially such that if an induced velocity at some radius is known, then the lift and drag forces at the blade element can be accurately predicted using the section lift and drag coefficient data, also known as airfoil polars. These airfoil polars are a function of Reynolds Number (Re) and Angle of Attack (AoA) and are obtained experimentally beforehand.

By combining MT and BET, it is possible to obtain induced velocities at various radii along the rotor plane at each blade element location, which fills the void when trying to accurately estimate the aerodynamic forces and induced velocities of a rotor. This means that CFD codes can calculate all source terms across a rotor accurately without ever prescribing any three-dimensional (3D) geometry to the rotor blade region. The lack of a resolved geometry in this region means that the simulation can produce data at an acceptable fidelity with a lower resolution mesh, hence lowering the computational cost since there are less computations taking place. Also note that pure MT uses disc loading as the only design parameter, while BET introduces parameters like blade loading, chord distribution, sweep angle distribution, twist distribution, and blade airfoil characteristics. The coupled BEM approach, therefore, is particularly useful in aerodynamics design optimization since BEM is highly parameterized in comparison to simple MT. This approach has historically been used in the preliminary design of aircraft, but this work suggests that the same approach can be used in the context of bicycle wheels due to geometric similarities.

In the commercial code Star-CCM+, BEM can be implemented by adding a virtual disk model into the Physics continuum. A virtual disk is a simple interpolation grid that sits atop the finite volume mesh as shown in Figure 3. The size of this interpolation grid is configurable and is what determines the computational cost required to model the flow field across the rotor plane. In this example, the interpolation grid has a resolution of 18 by 3, consisting of 54 elements. The BEM approach in Star-CCM+ requires that each element contain at least one finite volume cell, therefore mesh optimization is necessary to lower computational cost effectively.
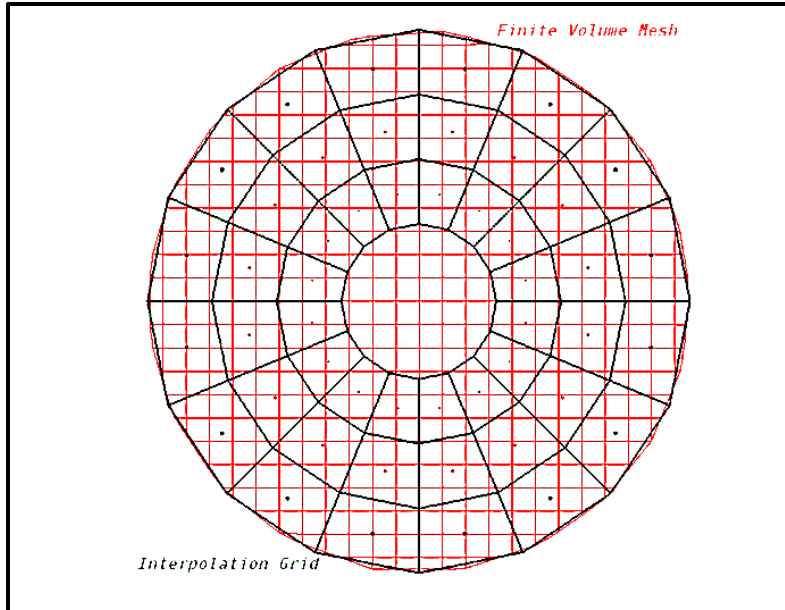
Figure 3: BEM Virtual Disk Interpolation Grid (Star-CCM+ User's Manual, 2020)

The BEM virtual disk can be given properties that reflect the rotor and blades true geometry. Once configured, the aerodynamic forces and induced velocities of the rotor are calculated by applying the BEM algorithm to the interpolation grid. The inflow angle is first calculated to obtain the AoA for finding induced velocities and forces:
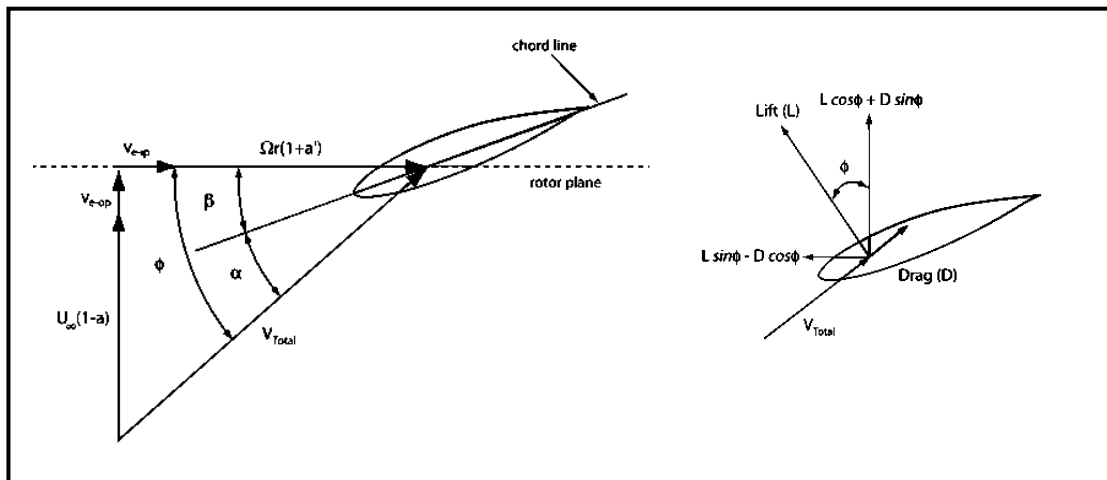
Figure 4: Local Elemental Velocities and Flow Angles, Local Elemental Forces, (Moriarty and Hansen, 2000)

Incorporating the 2D airfoil polars into the algorithm yields a set of equations that can be iteratively solved for the induced velocities and forces on each blade element. Tip-loss and other corrective models can be applied. An unsteady, also called time-accurate, version of the BEM algorithm exists but this work only deals with steady flow, so only the steady BEM algorithm is employed.

Limitations of BEM

No matter how complicated a model is in detail, it will still only represent a simplified picture of reality. Such is the case with BEM. While BEM has a history of effectively predicting the aerodynamics of rotors, one must be aware of the potential limitations of using a simplified model. Specifically for time-averaged BEM algorithms, limitations may arise due to the assumption of airflow being static while the wake is time-dependent by nature, and thus subject to transient fluctuations that take time for the airfoils respond to (Snel and Schepers, 1995). From the point of view of predicting the overall aerodynamics performances of a rotor, this limitation is not much of a concern; however, this means that the time-averaged BEM approach is limited to steady simulations and hence should be used with Reynolds Averaged Navier Stokes (RANS). Other limitations of the BEM model arise from losses at the rotor hub and blade tips. Original BEM algorithms did not account for the influence of blade tip vortex shedding, which causes a higher local inflow near the tip and effectively increases the lift capability in this region. Star-CCM+ features a built in tip-loss model that is configurable by the user, so this is also a non-issue. Tip-loss factor is specified as a function of the normalized disk span, which is given by:

$$r' = \frac{r}{R} \quad (1)$$

It is unknown whether or not a hub-loss model is built into Star-CCM+, but this can be

configured with custom user code if necessary. It is assumed for this work that no hub-loss is

present. This could be a topic for future works. In conclusion, BEM, from a theoretical point of

view, seems perfectly acceptable for this work since the authors are only concerned with the

overall aerodynamics performances of bicycle wheels at a steady state.

Chapter 3: Methodology

Bicycle Wheel Geometry

The HED Trispoke is chosen as the ideal test subject for two reasons: 1) it presents the ideal spoke geometry for the first experimentation with BEM and 2) there is an abundance of existing CFD and wind tunnel data available. As the name implies, the wheel has three spokes that have an aerodynamic shape resembling that of a NACA 0012 airfoil. The Trispoke has a long history in cycling, originally developed in 1998 in collaboration with DuPont. Cyclists quickly adopted the wheel for time trialing due to its claimed aerodynamic advantage at high speeds and low yaw angles.
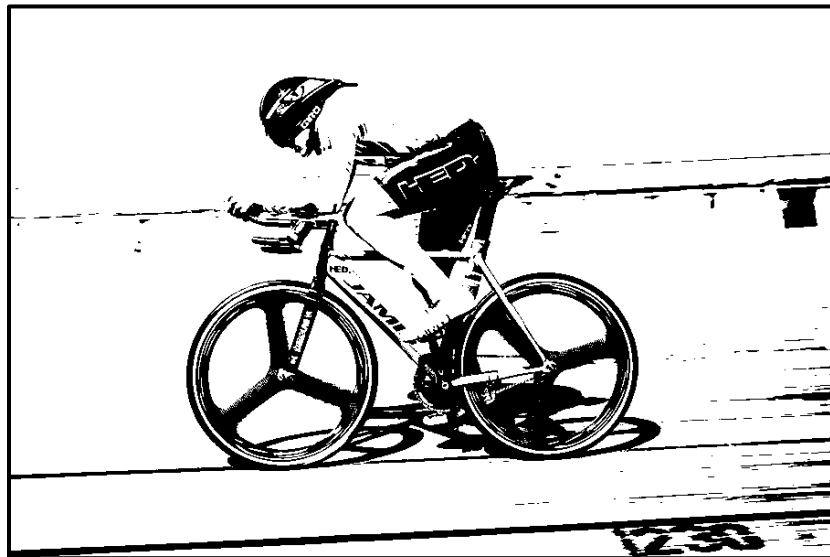
Figure 5: Time Trial Cyclist with HED Trispoke Wheels

The Trispoke's geometry is reverse engineered from images provided by HED and measurements found in previous works (Godo et al., 2010). The nominal diameter, D, is set to be 0.678m, a typical size for a 700C bicycle wheel. All other dimensions are set relative to D. A tire with a circular cross-section is also included in the rim geometry. During actual cycling

conditions, the tire would deform on the contact patch, but for simplicity this is neglected in the model. The rim and spokes are perfect replicas, but the hub is idealized to be a cylindrical disk. The wheel with resolved spokes of course requires 3D rim, hub, and spoke geometries; however, the wheel with modeled spokes only requires the 3D rim geometry since the spokes are modeled using a BEM virtual disk. This yields two models of the Trispoke that must be considered in this work. The naming convention is defined in Figure 6.
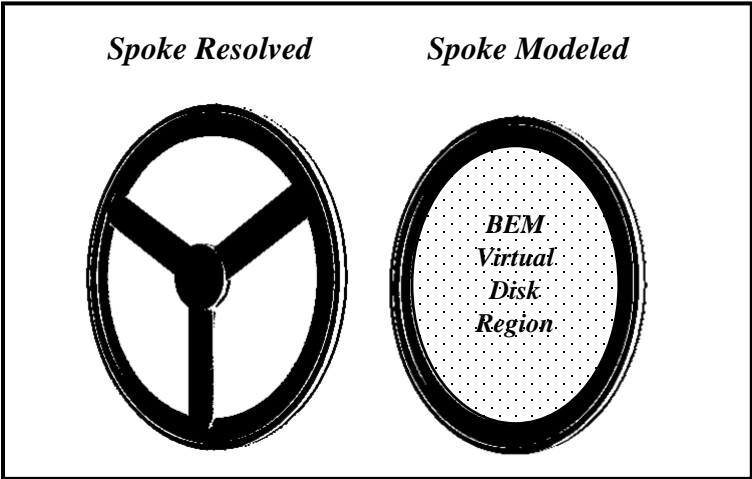
Figure 6: Spoke Resolved and Spoke Modeled Geometries
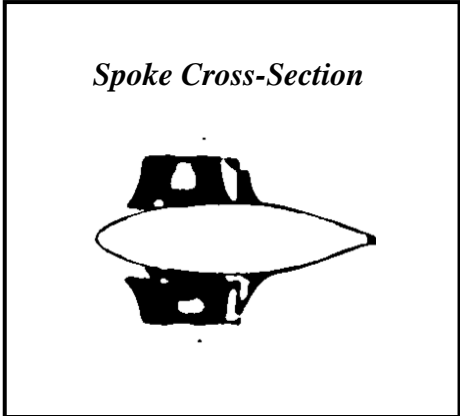
Figure 7: Cross-Section of the HED Trispoke Spoke Geometry

Airfoil Polar Generation

As stated in the previous chapter, BEM requires 2D airfoil polars to predict lift and drag forces on each of the blade elements. Ideally this data would be obtained experimentally from the wind tunnel, but in this work CFD is used and will suffice. Figure 7 shows the cross-section of the HED Trispoke spoke geometry, which is used to reverse engineer a 2D computational grid with a normalized chord length. The spoke is meshed with an overset mesh, which then sits within the rectangular domain. Symmetry plane boundary conditions are applied to the top and bottom boundaries. A velocity inlet and an extrapolated pressure outlet are applied to the left and right boundaries. Refinement was added to the wake region. The commercial code Star-CCM+ is used to solve steady state RANS equations along with the single-equation Spalart-Allmaras (SA) turbulence model. These equations will be further discussed in later chapters.
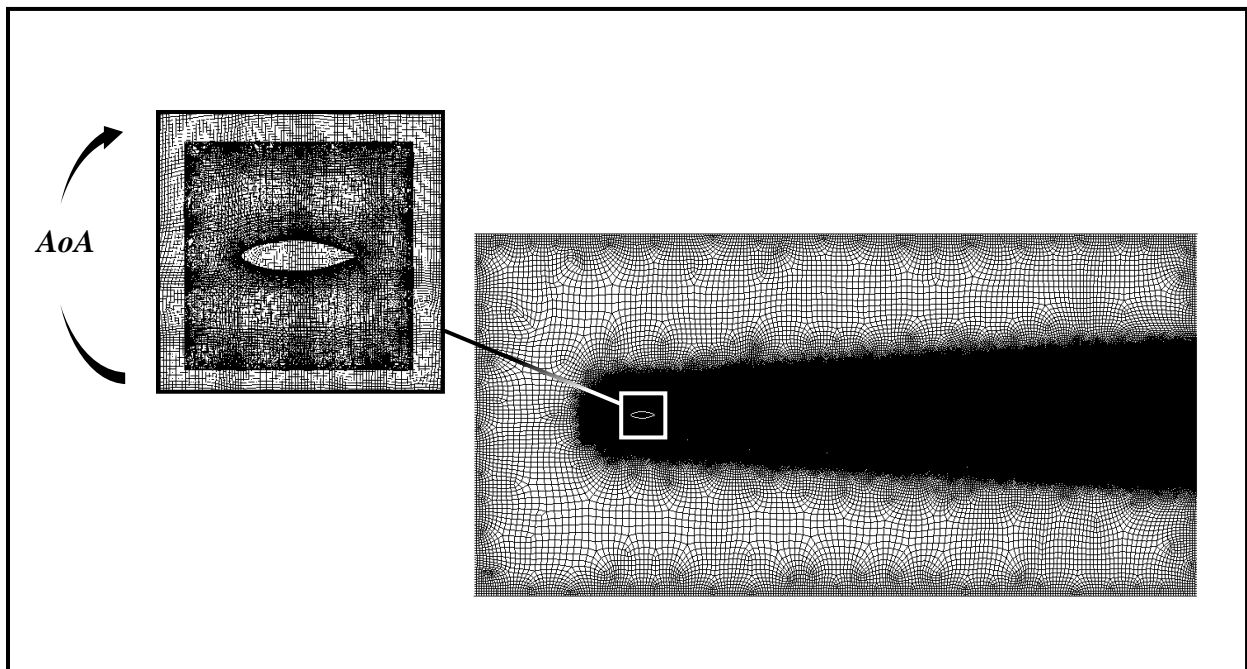
Figure 8: Exploded View of Spoke Overset Mesh and Computational Grid

Star-CCM+ Design Manager is used to create 1500 CFD simulations of the 2D HED Trispoke Spoke geometry in order to generate its 2D airfoil polars. The overset mesh is allowed to rotate from 0 degrees to 180 degrees at a step size of 3 degrees as shown in Figure 8. This is accomplished using Java macros. The velocity inlet is allowed to vary with Re ranging between 100k and 500k at a step size of 20k. Due to the range of Reynolds numbers, flow is assumed to be incompressible at constant density and therefore the segregated flow model is used. Each simulation is run on a Linux cluster with 12 computational cores, and the Star-CCM+ log files are saved for post-processing with Python.

Figure 9: Drag Coefficient and Lift Coefficient of 2D HED Trispoke Spoke at Re = 100k, AoA = 135 Degrees
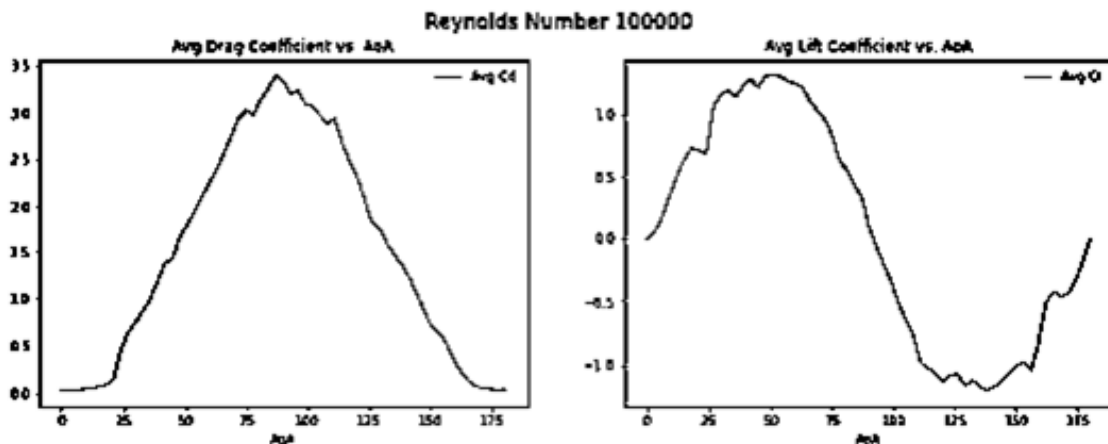
Figure 10: Airfoil Polar (Cd vs. AoA and Cl vs. AoA) of 2D HED Trispoke Spoke at Re = 100k

Figure 9 demonstrates how the Python code parses though all 1500 simulation log files and plots raw drag and lift coefficients vs. iteration. Past the critical AoA, such as in Figure 9 where AoA is 135 degrees, oscillating solutions are to be expected. To account for these oscillations, an averaging algorithm is applied to estimate average drag and lift coe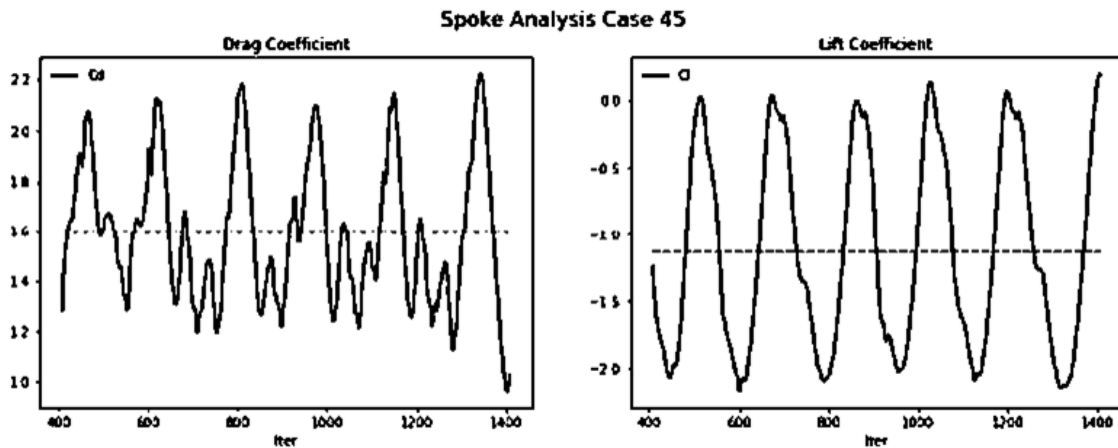fficients at each Reynolds number and AoA (illustrated by the dotted lines in Figure 9). Figure 10 demonstrates how each airfoil polar is generated using this averaged data for all Reynolds numbers and AoA combinations. The final results are tabulated and stored in a csv as shown in Table 1.

Cd	Cl	Re	AoA (rad)
0.029896	0.000770	100000	0.000000
0.031243	0.055721	100000	0.052360
0.035186	0.180837	100000	0.104720
0.041788	0.340806	100000	0.157080
0.051848	0.500801	100000	0.209440
0.066776	0.638372	100000	0.261800
0.089609	0.727475	100000	0.314159
0.137266	0.715882	100000	0.366519
0.443502	0.681876	100000	0.418879
.	.	.	.
.	.	.	.
.	.	.	.
0.001441	0.000007	500000	3.141594

Table 1: Tabulated Airfoil Polars for 2D HED Trispoke Spoke

Computational Domain

As mentioned previously, two CFD simulations are considered: 1) Spoke Resolved, which uses fully resolved spokes and 2) Spoke Modeled, which uses modeled spokes using a BEM virtual disk. Each use equally dimensioned computational domains with identical boundary conditions, which are similar to computational domains and boundary conditions found in previous bicycle wheel CFD works (Godo et al., 2009; Godo et al., 2010; Godo et al., 2011). A velocity inlet supplies a constant flow of air, V_e, which varies depending on the yaw angle. An extrapolated pressure outlet is used. A no-slip ground plane is set to translate at the effective velocity, V_e. Slip symmetry planes were used for the top and side planes. The wheel is set to rotate at a rate of w as if it were translating on a bicycle travelling at a velocity, V, using a rotating reference frame surrounding the wheel region.
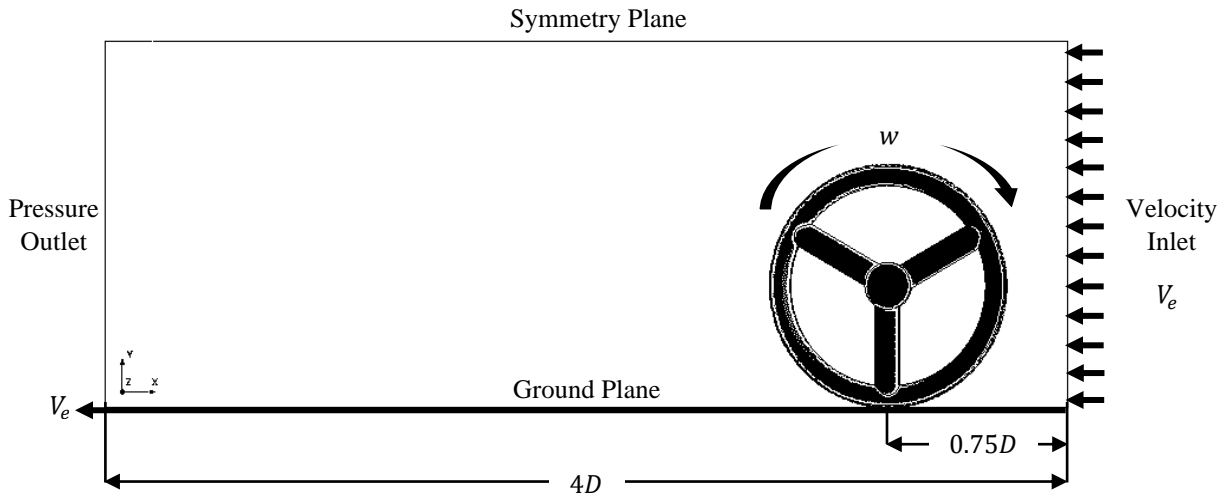

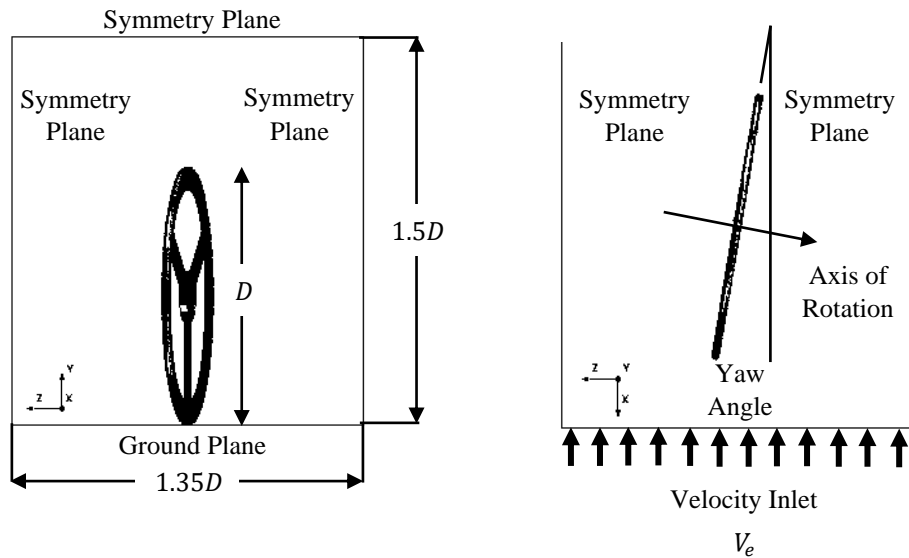Figure 11: X-Y Axis of Computational Domain with Boundary Conditions

Figure 12: Y-Z (Left) and X-Z (Right) Planes of Computational Domain with Boundary Conditions

When calculating resolved forces, a local coordinate system relative to the wheel is such that the positive X-Axis is perpendicular to the wheel's axis of rotation and is pointing upstream, the positive Z-Axis is parallel but pointing opposite to the axis of rotation, and the Y-Axis is pointing upwards towards the top symmetry plane. This coordinate system is x', y', and z'.

Numerical Methods

A time-averaged CFD approach is used to calculate the flow field around the HED Trispoke wheel by solving the RANS equations with a single-equation SA turbulence model. The SA equations provide closure to the RANS equations by solving the transport equation for the modified diffusivity, $\tilde{v}$, in order to determine the turbulent eddy viscosity. SA is a low Reynolds number model so it is applied without any wall functions. This means that the entire turbulent boundary layer, including the viscous sublayer, can be accurately resolved in fine meshes where y^+ values are small. Therefore, it is important to include sufficiently small prism layers when meshing. SA is generally a good choice when the boundary layers are mostly

attached with mild separation (i.e., low Reynolds number external flows like flow around a bicycle wheel). The following Navier-Stokes equations are solved using Star-CCM+:

$$\frac{\partial \rho}{\partial t} + \nabla \cdot \rho u = 0 \quad (2)$$

$$\rho \frac{\partial u}{\partial t} + \rho u \cdot \nabla u + \nabla p = \nabla \cdot T + \rho b \quad (3)$$

Where p = pressure, T = viscous stress tensor, b = momentum source vector, and u = velocity vector. The SA turbulence equation is as follows:

$$\frac{\partial \tilde{v}}{\partial t} + u \cdot \nabla \tilde{v} = c_{b1}\tilde{S}\tilde{v} - c_{w1}f_w \left(\frac{\tilde{v}}{d}\right)^2 + \frac{1}{\sigma}\left[\nabla \cdot \left((v + \tilde{v})\nabla \tilde{v}\right) + c_{b2}(\nabla \tilde{v})^2\right] \quad (4)$$

Where $\tilde{v}$ = modified diffusivity, d = length scale, $c_{b1} = 0.1355$, $c_{b2} = 0.622$, $c_{w1} = \frac{c_{b1}}{k^2} + \frac{1+c_{b2}}{\sigma}$, $c_{w2} = 0.3$, $c_{w3} = 2.0$, and $c_{v1} = 7.1$. The aforementioned SA variables are standard in Star-CCM+. Finally, flow is assumed to be incompressible and constant density due to the range of Reynolds numbers, therefore the segregated flow model is used. At high yaw angles some SA under-relaxation is required for convergence.

Mesh Refinement Study

A grid density study consisting of 6 grid density levels ranging from 200 thousand to 6.4 million cells is performed on both Spoke Modeled and Spoke Resolved simulations, so 12 simulations were run in total using Star-CCM+ Design Manager on a Linux cluster with 12 computational cores. The study is limited to the HED Trispoke wheel at a critical yaw angle of 10 degrees with the wheel rotating and ground translating as if the cyclist is moving at 30 mi/h. The solution is considered converged when there was less than a 5 percent change between drag coefficient values.

Drag Coefficient vs. Grid Density		
	Cd	*Number of Cells (Million)*
Spoke Modeled		
Design 1	0.036	0.21
Design 2	0.028	0.57
Design 3	**0.026**	**1.32**
Design 4	0.026	2.41
Design 5	0.024	4.15
Design 6	0.022	6.36
Spoke Resolved		
Design 1	0.035	0.21
Design 2	0.027	0.58
Design 3	0.033	1.30
Design 4	**0.023**	**2.37**
Design 5	0.022	4.18
Design 6	0.022	6.39

Table 2: Mesh Refinement Study of Drag Coefficient vs. Grid Density

A relatively small computational grid consisting of 1.32 million cells is considered sufficiently converged for the Spoke Modeled simulation. A relatively larger computational grid consisting of 2.37 million cells is required to achieve a sufficient level of convergence for the Spoke Resolved simulation. Spoke Modeled is able to employ a less refined mesh in the spoke region since the spokes are being modeled using BEM for reasons discussed earlier. The region where the spokes are in the Spoke Modeled case still has a fine enough mesh for a BEM virtual disk with a 50 by 50 resolution, which yields an interpolation grid containing 2500 elements. It is important to note that the goal with this mesh refinement study is to compromise between simulation fidelity and computational cost. In other words, this mesh resolution is not intended to achieve the highest fidelity possible, but rather a satisfactory fidelity that produces CFD in good agreement with existing CFD and wind tunnel data.

Chapter 4: Results and Discussion

Comparison Between Methods

The aerodynamics of the HED Trispoke are predicted at various yaw angles ranging from 0 to 20 degrees in increments of 5 for both Spoke Modeled and Spoke Resolved simulations, so 10 simulations in total are run on a Linux cluster with 12 computational cores. The wheel is rotating and the ground is translating as if the cyclist was moving at 30 mi/h. Results of Spoke Modeled and Spoke Resolved are compared between each other.
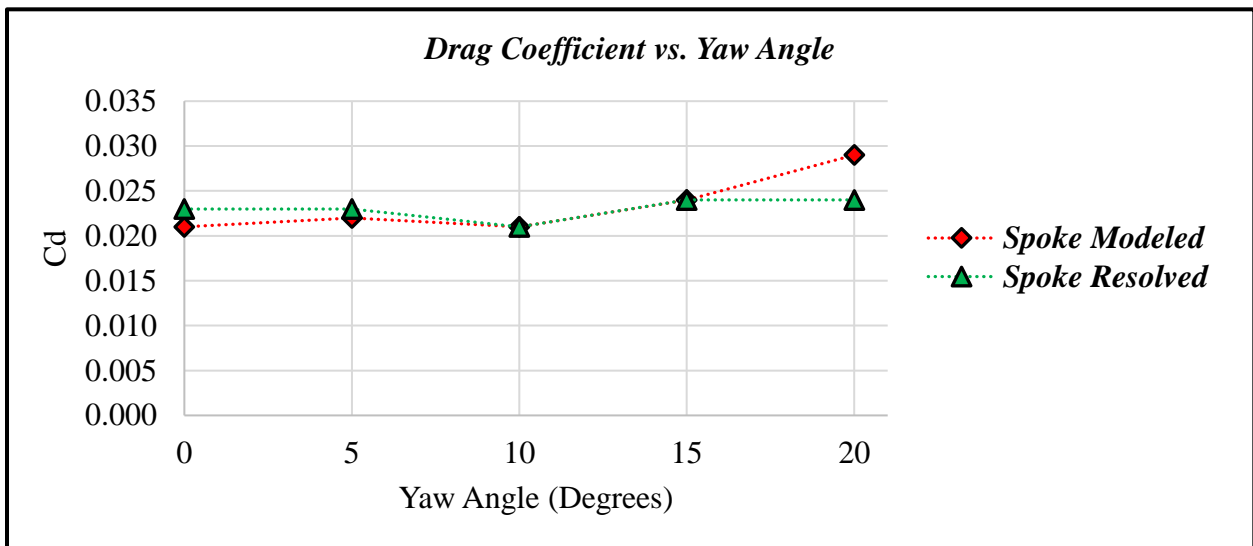

Figure 13: Drag Coefficient vs. Yaw Angle for Spoke Modeled and Spoke Resolved

Drag coefficient data from Spoke Modeled simulations appear to be in good agreement with drag coefficient data from Spoke Resolved simulations, particularly at yaw angles between 0 and 15 degrees. Spoke Modeled slightly overestimates drag coefficient at the 20 degree yaw angle by 9 percent. According to Figure 15, the source of this discrepancy could be from the slight overprediction of drag force by Spoke Modeled.
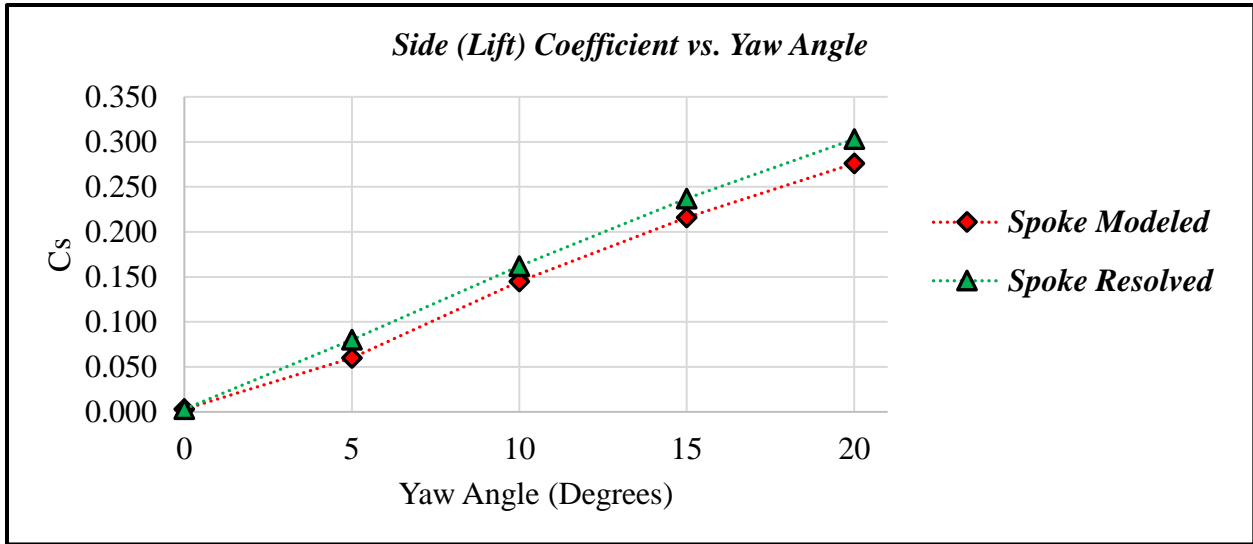
Figure 14: Side (Lift) Coefficient vs. Yaw Angle for Spoke Modeled and Spoke Resolved

Side (lift) coefficient data shows strong agreement in between the Spoke Modeled and Spoke Resolved cases with the modeled spokes only slightly underestimating lift. The general trend appears to be an increasing linear relationship between lift and yaw. The linear trendline for Spoke Modeled has a slope of 0.014 while Spoke Resolved has a slope of 0.015, so this relationship is nearly identical between the two cases.
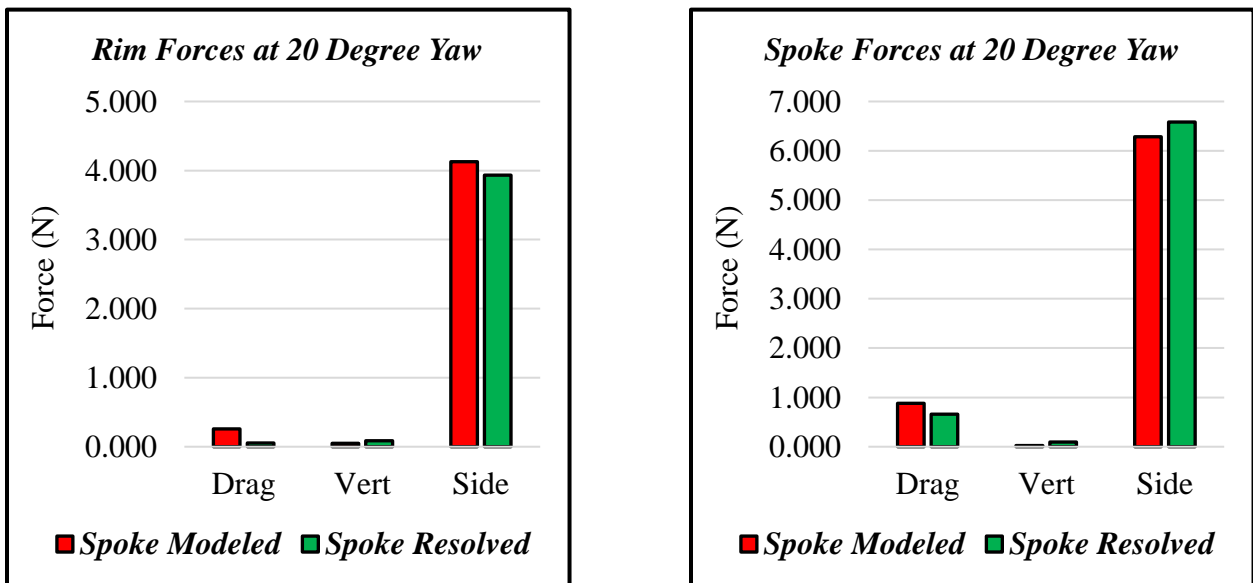

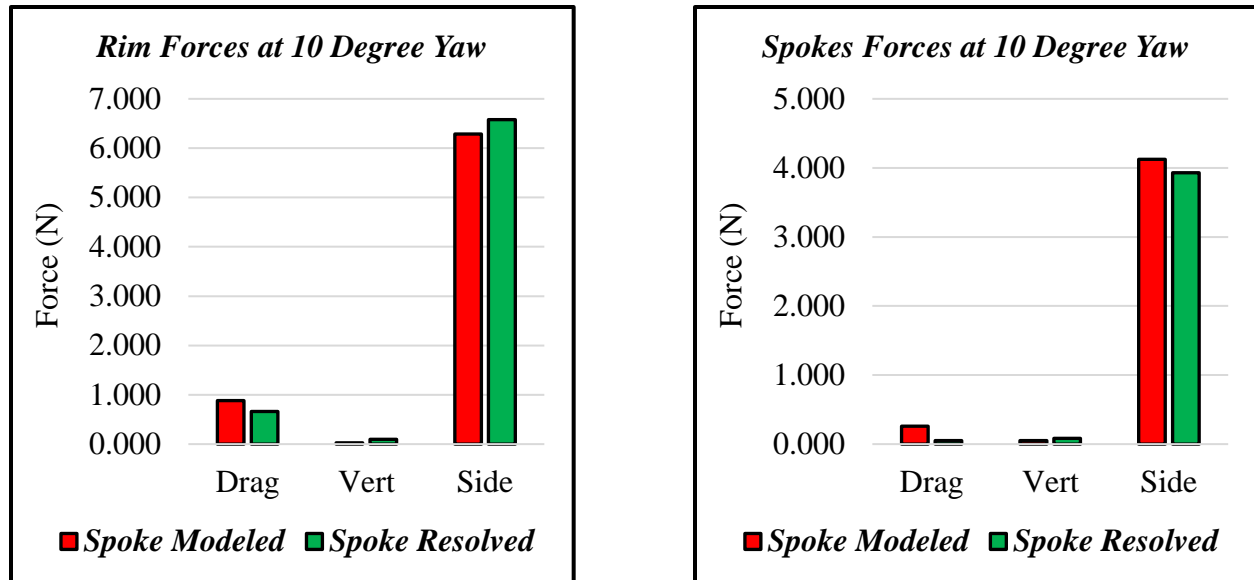Figure 15: Comparison of Force Components at 20 Degree Yaw Angle

Figure 16: Comparison of Force Components at 10 Degree Yaw Angle

Figures 15 and 16 demonstrate strong agreement between Spoke Modeled and Spoke Resolved. The magnitudes of the rim and spoke induced forces are relatively close in proximity and show matching trends.

It has been established that the purpose of this work is to lower the computational cost of CFD involving bicycle wheels by applying BEM to the spokes, which requires a less refined computational grid and thus requires less time to solve. The computational grid used for Spoke Modeled contains 1.32 million cells whereas that of Spoke Resolved contains 2.37 million cells. Convergence is generally achieved by the 300th iteration, so computational time will be determined by the amount of time it takes for each simulation to reach 300 iterations. All settings of Spoke Modeled and Spoke Resolved are identical except for the computational grid. For each simulation, Star-CCM+ is used to solve the flow field around the HED Trispoke wheel models using 10 computational cores on a Linux cluster.

Comparison of Computational Time			
Time (s)			
Yaw Angle (Degrees)	Spoke Modeled	Spoke Resolved	Percent Difference
0	263	497	89
5	251	493	96
10	255	499	96
15	258	491	90
20	257	496	93
Avg. Percent Diff.	93		

Table 3: Comparison of Computational Time Between Spoke Modeled and Spoke Resolved

On average, Spoke Modeled is able to compute the flow field around a HED Trispoke wheel in 93% less time compared to Spoke Resolved. This is a significant reduction in computational time while data fidelity remains good. There are some discrepancies between Spoke Modeled and Spoke Resolved that must be noted, such as the 9 percent overprediction in drag at 20 degree yaw as well as some individual force components showing slight deviations.
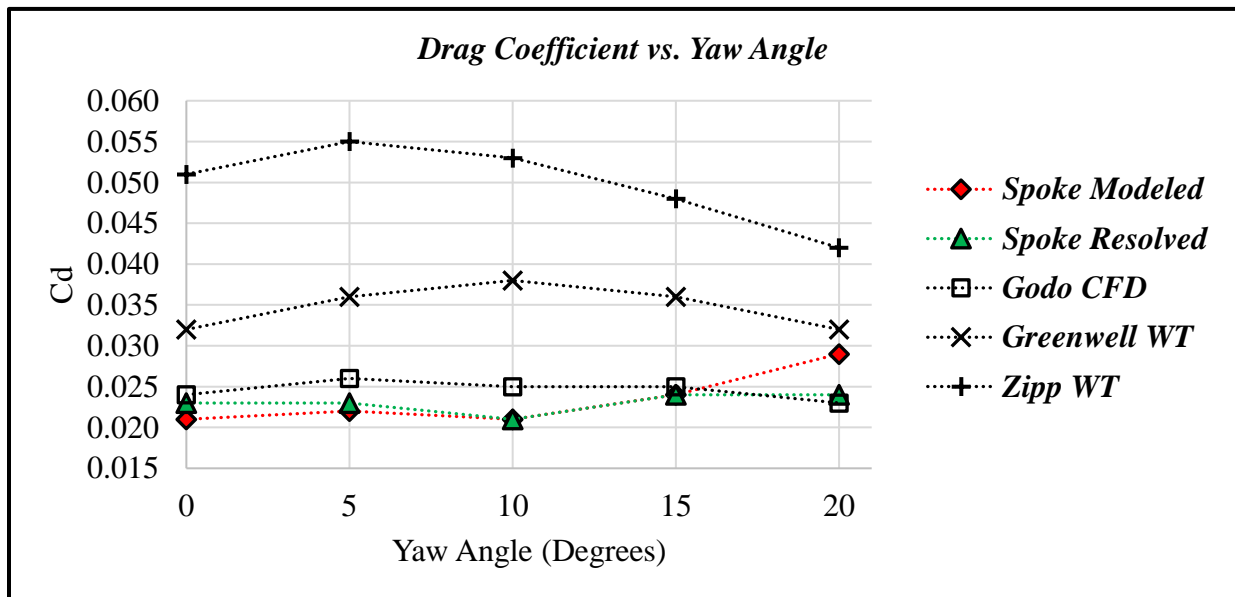
Comparison to Existing Data

Figure 17: Drag Coefficient vs. Yaw Angle Comparison

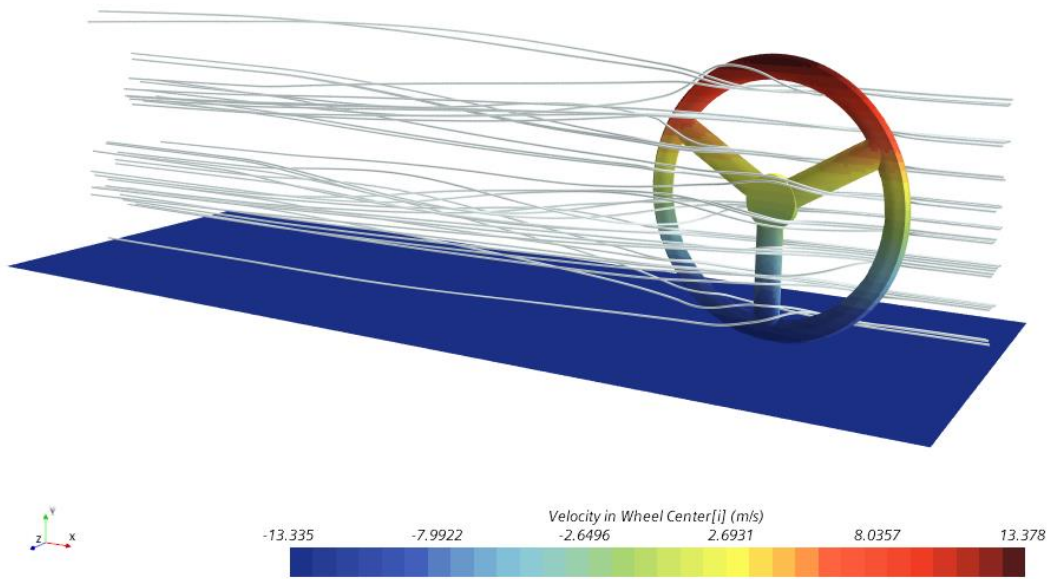**Spoke Modeled vs. Spoke Resolved Streamlines**

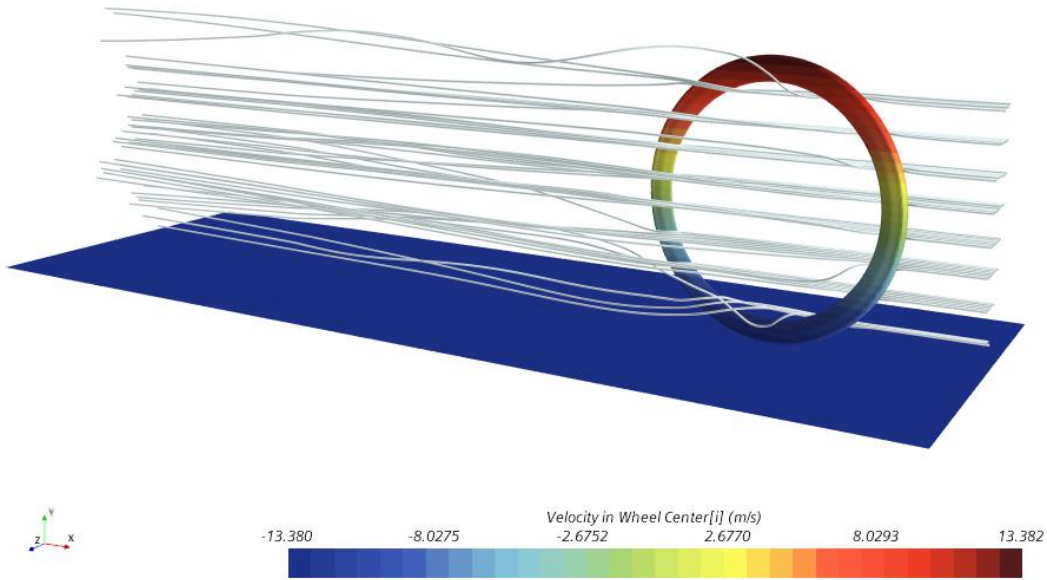Figure 18: Spoke Resolved Streamline Scene

Figure 19: Spoke Modeled Streamline Scene

Streamlines in Spoke Modeled appear healthy albeit are lacking high resolution turbulence that is found in Spoke Resolved; however, this is to be expected with the time-averaged BEM model.

Chapter 5: Conclusion and Future Works

Drag coefficient data for Spoke Modeled and Spoke Resolved appears to be in good agreement with each other and with existing CFD and wind tunnel data, although Spoke Modeled slightly overpredicts drag coefficient at 20 degrees of yaw by 9 percent. Side coefficient data in between Spoke Modeled and Spoke Resolved is in strong agreement, displaying matching linear trends such that lift increases as yaw increases. Force decomposition charts show strong correlations between methods, with Spoke Modeled having rim and hub component forces with relatively similar magnitudes compared to Spoke Resolved. Spoke Modeled is able to accomplish this at a 93% reduction in computational cost.

This work shows promising results for using BEM in the context of a bicycle wheel; however, future works are necessary before employing the model in industry. Some tweaking of the BEM model should be made to include hub-losses and perhaps a hub model since Star-CCM+ does not appear to employ such a thing. Some BEM algorithms, like AeroDyn has hub-loss corrections built in so this is possible. The BEM model should also be employed for other wheel geometries such has the Zipp 404 wheel with Sapim racing spokes (small elliptical spokes, 24 of them typically). This would further validate the model as a general tool for all types of bicycle wheels.

As mentioned previously, one of the attractive features of BEM is high parameterization, which makes for easy preliminary design analysis of rotor aerodynamics. The authors believe that this tool could be used to rapidly iterate over several wheel and spoke design combinations to converge to an ideal bicycle wheel geometry. This would mean the cycling industry could adopt the BEM approach for bicycle wheel design similar to how the aerospace industry has adopted it for wind turbine and helicopter rotor design.

REFERENCES

1. GRAPPE, FREDERIC, et al. "Aerodynamic Drag in Field Cycling with Special Reference to the Obree's Position." *Ergonomics*, vol. 40, no. 12, 1997, pp. 1299–1311.

2. Kyle, Chester R., and Edmund Burke. "Improving the racing bicycle." *Mechanical engineering* 106.9 (1984): 34-45.

3. Greenwell, D. I., et al. "Aerodynamic characteristics of low-drag bicycle wheels." *The Aeronautical Journal* 99.983 (1995): 109-120.

4. Godo, Matthew, David Corson, and Steve Legensky. "An aerodynamic study of bicycle wheel performance using CFD." *47th AIAA Aerospace Sciences Meeting Including The New Horizons Forum and Aerospace Exposition*. 2009.

5. Godo, Matthew, David Corson, and Steve Legensky. "A comparative aerodynamic study of commercial bicycle wheels using CFD." *48th AIAA Aerospace Sciences Meeting Including the New Horizons Forum and Aerospace Exposition*. 2010.

6. Godo, Matthew, David Corson, and Steve Legensky. "A practical analysis of unsteady flow around a bicycle wheel, fork and partial frame using CFD." *49th AIAA Aerospace Sciences Meeting including the New Horizons Forum and Aerospace Exposition*. 2011.

7. Debraux, Pierre, et al. "Aerodynamic drag in cycling: methods of assessment." *Sports Biomechanics* 10.3 (2011): 197-218.

8. Yaggy, P., Dat, R., Fabre, P., Harris, F., Lowson, M. V., Mckenzie, K. . T., Reichert, G., Huber, H., & Stepniewski, W. Z. (1973). *AGARD LECTURE SERIES No. 63 on Helicopter Aerodynamics and Dynamics*. *63*.

9. Moriarty, Patrick J., and A. Craig Hansen. *AeroDyn theory manual*. No. NREL/TP-500-36881. National Renewable Energy Lab., Golden, CO (US), 2005.

10. Snel, H.; Schepers, J.G. (ed.) 1995. Joint Investigation of Dynamic Inflow Effects and Implementation of an Engineering Method. ECN-C-94-107, Petten: Energy Research Centre of the Netherlands April.